Electric Field Induced Assembly of Vimentin Microscaffolds around Metallic Electrodes

Terry R. Colbourne, Ian G. Hill, and Laurent Kreplak*

Department of Physics and Atmospheric Science, Dalhousie University, Halifax, NS, B3H 3J5, Canada

Received April 8, 2009; Revised Manuscript Received May 28, 2009

The self-assembly properties of fibrous proteins such as collagen are frequently used to form three-dimensional scaffolds. In this study we investigated the effect of nonuniform alternating and static electric-fields on the self-assembly properties of a dilute solution of vimentin. In the presence of both types of fields at the same time, vimentin was observed to accumulate at the positive electrode and to form microscaffolds bridging the two electrodes in 20−30 min. Atomic force microscopy of the surface of dried microscaffolds revealed the presence of dense 8−12 nm diameter vimentin filament meshworks as well as bundles with typical diameters of 100−200 nm. Stretching of the scaffolds revealed that either the bundles or drawn meshworks could be extended to at least 6-fold and the presence fibers with a width of several μm.

Introduction

Dielectrophoresis (DEP) is commonly employed in microfluidic devices to manipulate and concentrate μm-sized particles such as colloids[1] or cells.[2,3] The movement is induced by a nonuniform electric field due to polarization effects. DEP can be induced both by alternating (AC)[4] and by direct (DC)[5] fields. In the case of polymers or biomacromolecules such as DNA or proteins that have dimensions in the nanometer range, DEP can also be employed to achieve higher local concentration than in the bulk.[6−8] However, in all these cases, the concentration gradient is dependent on the electric field and can be destroyed by thermal fluctuations under zero field.

Let us consider a special case where the biomacromolecules have the tendency to self-assemble into filaments or fibrils at a given pH and ionic strength. Fibrous proteins such as collagen, fibrinogen, and elastin and all the intermediate filament (IF) proteins belong to this subgroup of proteins.[9] If a concentration gradient is imposed in the assembly regime, one would expect the formation of a gel or web-like structure that would persist even under zero field. To test this hypothesis we selected the IF protein vimentin for which the assembly pathway is well characterized.[10−12] At low ionic strength and high pH, vimentin forms a tetramer 70 nm in length and 2−3 nm in diameter.[11,13] When the pH is switched to 7.5 and the ionic strength is increased to 100 mM or more, assembly is initiated.[10] The first step is the formation of unit-length filaments (ULFs) 60 nm in length and 15 nm in diameter that contain eight tetramers in each cross-section or more.[10] This step is almost complete within seconds and the remaining process occurs over the course of an hour at protein concentrations in the μM range. The second step is the end to end fusion of the ULFs into filaments that finally compact to form smooth-looking, 10 nm wide, μm long structures (Figure 1).[10,12,14] The assembly process has a temperature optimum at 37 °C for human vimentin, but the protein remains assembly competent at room temperature.[15] The filaments are very flexible, with a persistence length around 1 μm,[16] and tend to form entangled arrays (Figure 1). Due to their flexibility, vimentin filaments and other IFs are not observable by light microscopy unless they form fibers, micrometers in diameter, through bundling.[17]

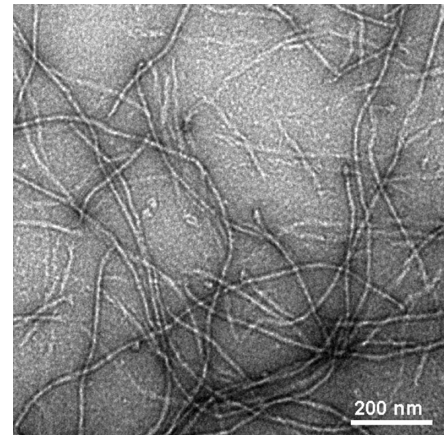

Figure 1. Electron microscopy picture of glutaraldehyde fixed vimentin filaments after 20 min of assembly at 37 °C. The vimentin concentration was 0.1 mg/mL.

In this study, we demonstrate that DEP, generated by a combined AC and DC field between two cylindrical electrodes facing end to end can concentrate vimentin in the vicinity of the electrodes in the assembly regime. We observed the formation of dense microscaffolds surrounding the electrodes that showed extreme extensibility before rupture. Atomic force microscopy imaging of dried microscaffolds revealed the presence of dense 8−12 nm diameter vimentin filament meshworks as well as bundles with typical diameters of 100−200 nm.

Materials and Methods

Vimentin Preparation. Human recombinant vimentin was obtained as described and stored at −80 °C in DP buffer (5 mM Tris-HCl, pH 8.4, 1 mM DTT) containing 8 M urea, 1 mM EDTA, 0.1 mM EGTA, and 10 mM methyl ammonium chloride.[14] The day before use, the protein was dialyzed in stepwise fashion at room temperature into DP buffer containing 6, 4, 2, and 0 M urea. Dialysis was continued overnight at 4 °C into fresh DP buffer without urea. Under this regimen, vimentin forms stable tetramers as previously demonstrated by analytical

* To whom correspondence should be addressed. Tel.: + 1 902 494 84 35. Fax: + 1 902 494 51 91. E-mail: kreplak@dal.ca.

10.1021/bm900398n CCC: $40.75
Published on Web 06/17/2009

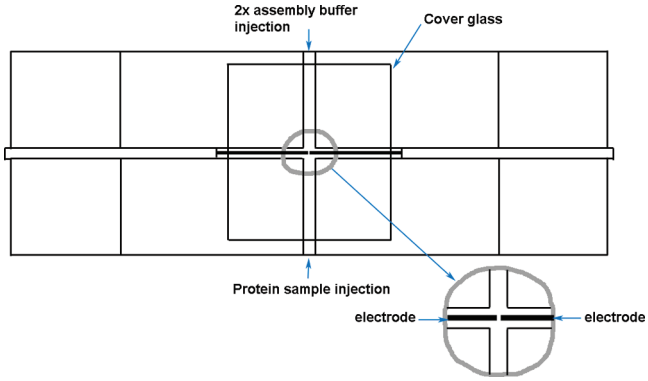

Figure 2. Sketch of the flow chamber used in this study.

ultracentrifugation.[11] Dialyzed protein was stored at 4 °C until used in an experiment. Unused protein was discarded after one week from the time of dialysis. Typical tetramer concentration varied from 0.20−0.50 mg/mL following dialysis as determined through UV−vis spectroscopy.

Dielectrophoresis Setup. For each experiment a flow-chamber was assembled as follows. Standard microscopic glass slides were cut into four 12 mm wide strips. Four strips were wiped clean with ethanol and glued with 5 min bonding epoxy to form a cross-pattern with a width of 1 mm on the glass slide (Figure 2). The open device was sonicated for 15 min in distilled water and blown dry. Then a clean cover slide was centered and glued over the cross with 5 min bonding epoxy to create a four-channel flow chamber (Figure 2). Electrodes of unwound Teflon-insulated silver-plated copper wire, 140 μm in diameter, were fixed into the two opposite long channels (Figure 1) at a distance of approximately 50−200 μm. The flow chamber was mounted on the stage of a BH2 Olympus microscope equipped with a dark-field condenser and a Canon EOS 450D digital camera. Electrodes were then connected to a potentiostat model 273 (Princeton Applied Research) associated with a Solartron 1255 frequency response analyzer (Schlumberger) to apply both AC and DC bias. Images were acquired every five seconds throughout an assembly experiment.

A 30 μL aliquot of a prepared 2× assembly buffer containing 40 mM Tris-HCl (pH 7.0), 200 mM NaCl and a 30 μL aliquot of dialyzed protein in DP buffer were heated to 37 °C for five minutes. The AC voltage and DC bias of the electrodes were then set on the impedance spectrometer and the image capture was initiated. Using two p200 pipettes, the warmed assembly buffer and protein were then advanced along the opposing channels perpendicular to the electrodes by capillary action before being simultaneously injected into the channels thus ensuring that both aliquots met near the electrode gap. Mixing was tested by replacing the protein by ink in the DP buffer. Complete mixing was observed within the first few seconds after injection (data not shown). We used a fine thermocouple to check the temperature inside the flow-chamber in the presence of AC voltage, DC bias and 20 watts of dark-field illumination. The temperature remained constant at 25 ± 1 °C. We also checked that the pH remained constant inside the flow-chamber for DC bias smaller than 2 V using 0.001% phenol red in 25 mM Tris-HCl (pH 7.5), 100 mM NaCl.

In some cases the obtained microscaffold was stretched by manually moving one wire while the other one remained in place. This enabled us to estimate the extensibility of the microscaffolds. In order to analyze the ultrastructure of the microscaffolds, we let them dry inside the chamber. They generally formed a strong bond to either the slide or the coverslip. After removal of the wires, the microscaffolds were recovered from the chamber, washed in ultrapure water to rinse any salt deposit, and dried with N_2.

Electron Microscopy. Aliquots of 20 μL were prepared by mixing equal volumes of vimentin tetramers in DP buffer at a concentration of 0.2 mg/mL with a 2× assembly buffer containing 40 mM Tris-HCl (pH 7.0), 200 mM NaCl. The assembly was carried out at 37 °C for up to one hour and terminated by adding 40 μL of 0.2% glutaraldehyde in water. The obtained filament solution was adsorbed onto a carbon coated copper grid and stained with 4% uranyl acetate. Images were acquired with a Hitachi 7500 transmission electron microscope operating at 80 keV.

Atomic Force Microscopy. Remnants of microscaffolds attached to glass were imaged by AFM in air. We acquired images in contact mode at a scan rate of 1−2 Hz using an Agilent 5500. The cantilevers were silicon nitride MSCT (Veeco, U.S.A.) with a nominal spring constant of 1.5 N/m.

Results

To assemble vimentin into filaments, we use a two-component system comprising equal volumes of a dilute vimentin solution at high pH and low ionic strength and a neutral pH, high ionic strength buffer (see Materials and Methods).[18] For vimentin concentration below 1 mg/mL, such assembly conditions yield clear suspensions of filaments around 10 nm in diameter that are invisible by light microscopy but observable by electron microscopy (Figure 1). Because vimentin has a pI of 5.06, it is negatively charged, $q = -19e$, at neutral pH. Hence, we predicted that an electric field applied between two electrodes in close proximity (Figure 2) would have an optically detectable effect on vimentin assembly in our two component system. Using an AC voltage of 1 V amplitude at 100 kHz and a DC bias between 100 and 500 mV, we performed negative control experiments by replacing the vimentin solution by DP buffer and by replacing the 2× assembly buffer by DP buffer. In both cases the mixed solutions remained transparent as expected.

Electric-Field Effects on Vimentin Assembly. In the presence of a 100 mV DC bias between two silver-plated copper wires, 160 μm apart (Figure 3A), we observed the deposition of vimentin on the silver coating (Figure 3B, arrowheads and inset) of the wire held at a positive potential. The deposition was progressive over the first five minutes and nothing changed during the remaining 15 min of the experiment (Figure 3B). The same experiment was then carried out by combining a 100 mV DC bias with an AC voltage of 1 V amplitude at 10 kHz. In that case, the rim of the positive wire was completely covered 3 min after injection (Figure 4A), some deposition was also detectable on the opposite wire and a tail of particles flowing from the vimentin deposit was observed as well (Figure 4A, arrowheads). The vimentin deposit took 15 min to grow into a dense microscaffold contacting both wires (Figure 4B, Supporting Information Video). The flow of particles gave rise to elongated structures that could be vimentin bundles (Figure 4B). The bright regions of the microscaffold observed in dark-field corresponded to regions of high contrast in bright-field (Figure 4C). The obtained microscaffold could be approximated by a sphere of 150 μm radius. Interestingly, if all the vimentin, 8 μg, used in this experiment assembled into 10 nm wide filaments that concentrated until close-packed, they would fill a sphere of 250 μm radius and achieve a concentration of 100 mg/mL. This is assuming 32 vimentin molecules per cross-section, and a molecule's length within the filament of 45 nm.[19] In other words, a large fraction of the vimentin was concentrated in the vicinity of the electrodes due to the AC and DC electric fields. Reducing the total amount of vimentin in the flow chamber to 1 and 0.1 μg yielded vimentin deposition mainly onto the positive wire but no complete microscaffold. Hence, in the following experiments we kept the total amount of vimentin in the flow chamber around 10 μg. In this regime, we also observed the formation of a microscaffold originating mainly from the positive wire when the frequency was decreased to 100 Hz or increased to 100 kHz and 1 MHz. We repeated these experiments by increasing the DC bias up to 500 mV and we observed

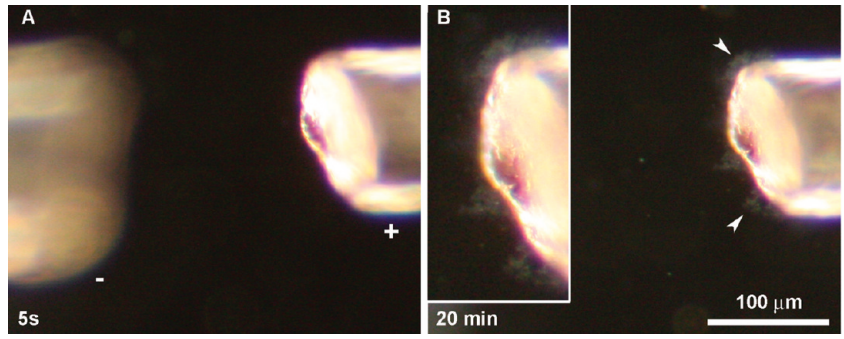

Figure 3. Mixing experiment in the flow chamber. The vimentin solution in DP buffer was at a concentration of 0.15 mg/mL. The wires had 100 mV DC bias and no AC voltage. (A) Dark-field image 5 s after injection of the two solutions. (B) Dark-field image 20 min after injection of the two solutions. Vimentin is deposited on the silver surface of the wire, at the edge with the copper core (arrowheads). Inset: the edge of the wire was blown up by a factor of 2.

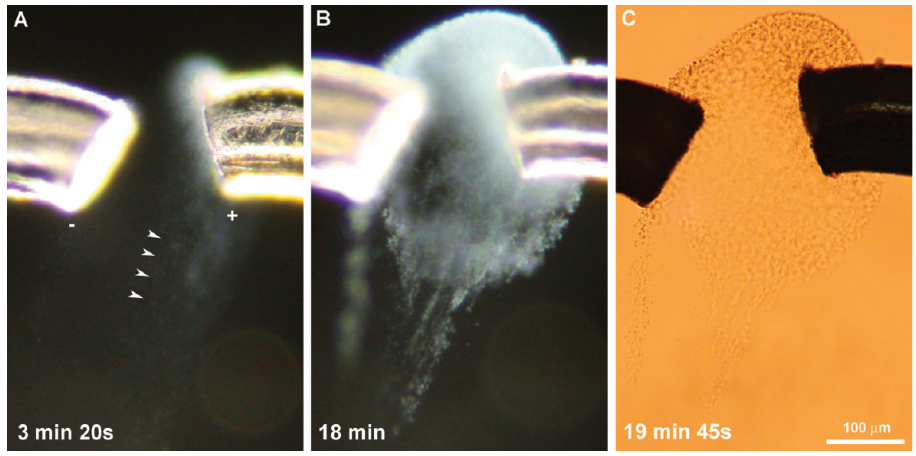

Figure 4. Mixing experiment in the flow chamber. The vimentin solution in DP buffer was at a concentration of 0.13 mg/mL. The wires had 100 mV DC bias and an AC voltage of 1 V amplitude at 10 kHz. (A) Dark-field image 3 min 20 s after injection of the two solutions. Growth is mainly visible on the positive wire as well as particles flowing away from the vimentin deposit (arrowheads). (B) Dark-field image 18 min after injection of the two solutions. A microgel has grown from the positive wire and filled the gap. (C) Bright-field image 18 min 45 s after injection. The microgel is transparent and regions of high contrasts correspond to regions of high scattering in the dark-field image.

a qualitative increase in microscaffold dimension with increasing DC bias (data shown). A summary of all the experimental conditions mentioned above is presented in Table 1.

We cyclically swept the frequency to 100 Hz, 1 kHz, 10 kHz, 40 kHz, and 100 kHz at 1 min intervals and observed a microscaffold as well (Figure 6A).

In order to understand the role played by the DC and AC parts of the electric field, we performed the following experiment with AC voltage of 1 V amplitude at 100 kHz. The DC bias was first fixed to +100 mV before injection and growth was observed on the positive wire for 8 min (Figure 5A). The DC bias was reduced to 0 mV and growth continued on the same wire for another 10 min (Figure 5B). Then the DC bias was fixed to −100 mV, and growth started on the opposite wire and continued for another 12 min (Figure 5C). Based on this sequence, it appears that the DC electric field is necessary for the initiation of protein deposition on the positive metallic surface, whereas the actual microscaffold growth is driven by the AC electric field. This was confirmed by the repeated observation that the AC electric field alone was not able to induce any vimentin deposition on the wires.

Extensibility of Vimentin Microscaffolds. In previous studies we have demonstrated that single intermediate filaments of the desmin, keratin, and neurofilament types can be extended up to 3.5× their original length.[20,21] At the macroscopic level, Hagfish slime threads that are 1 μm wide bundles of keratin-like filaments, exhibited an extensibility of 3.2× their original length.[22] The vimentin microscaffolds obtained in the presence of an electric field exhibit extreme extensibility as well (Figure 6). For example, a small microscaffold assembled by cyclically sweeping the frequency (see above) was stretched by increasing

Table 1. Experimental Conditions Allowing the Growth of Vimentin Microscaffolds

wire distance (μm)	vimentin concentration[a] (mg/mL)	DC bias (mV)	AC frequency[b] (kHz)
115	0.13	100	0.1
60	0.23	100	1
130	0.13	100	1
50	0.23	300	10
120	0.12	100	10
155	0.13	100	10
115	0.10	250	100
125	0.23	400	100
280	0.12	230	100
90	0.15	200	100
190	0.15	200	100
185	0.20	440	100
200	0.20	100	100
200	0.20	500	100
115	0.02[c]	100	100
135	0.002[c]	100	100
180	0.12	270	1000
145	0.13	100	1000

[a] The total volume injected inside the flow-chamber was 60 μL for all experiments. [b] Amplitude 1 V for all experiments. [c] Growth observed on postive electrode only.

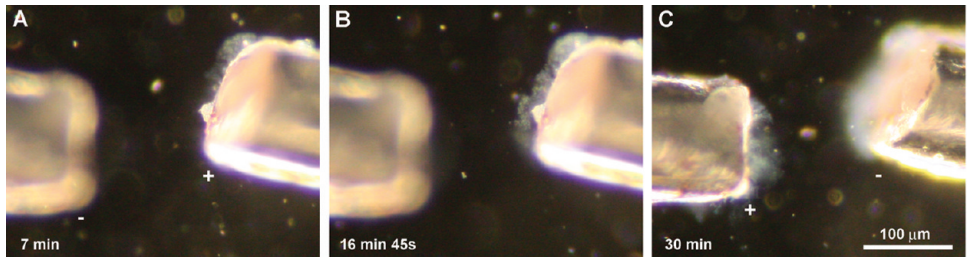

Figure 5. Mixing experiment in the flow chamber. The vimentin solution in DP buffer was at a concentration of 0.15 mg/mL. The wires had 100 mV DC bias and an AC voltage of 1 V amplitude at 100 kHz. (A) Dark-field image 7 min after injection of the two solutions. Growth is visible on the positive wire. (B) Dark-field image 16 min 45 s after injection of the two solutions. A total of 8 min after injection the DC bias was reduced to zero and growth proceeds on the previously positive wire. (C) Dark-field image 30 min after injection. A total of 18 min after injection we reversed the polarity of the wires and applied 100 mV DC bias again. Growth was observed on the newly positive wire.

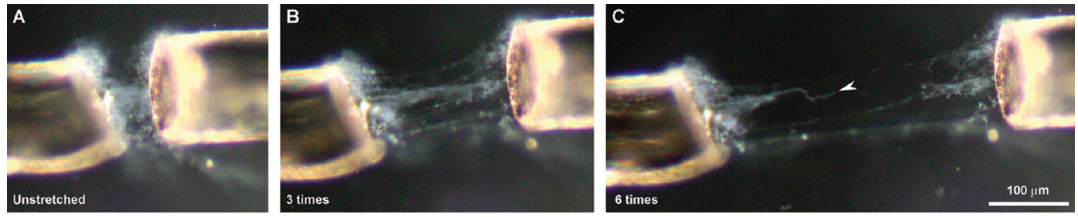

Figure 6. Mixing experiment in the flow-chamber. The vimentin solution in DP buffer was at a concentration of 0.1 mg/mL. The wires had 100 mV DC bias and an AC voltage of 1 V amplitude. The frequency was swept cyclically to 100 Hz, 1 kHz, 10 kHz, 40 kHz and 100 kHz at 1 min intervals. (A) Dark-field image 20 min 40 s after injection of the two solutions. (B) Dark-field image after increasing the gap between the two wires 3×. (C) Dark-field image after increasing the gap between the two wires 6×. One of the extended cable broke (arrowhead).

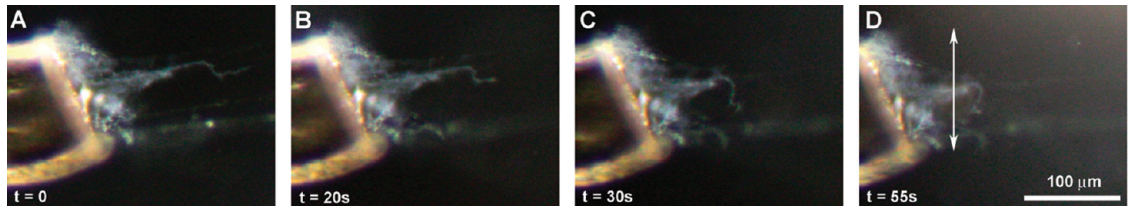

Figure 7. Relaxation of the extended cable that broke in Figure 6C: (A) breakage, (B) 20 s, (C) 30 s, (D) 55 s. The double arrow indicates the position of the second wire before stretching. Hence, the retraction is not complete after 55 s.

the gap between the two wires 3× (Figure 6B) and 6× (Figure 6C), respectively. Thin straight cables originating from the microscaffold were observed to extend between the two wires (Figure 6B,C). One of the cables broke during stretch (Figure 6C, arrowhead) and appeared to coil back without retracting completely over the course of 55 s (Figure 7). The fact that the retraction was not complete after this time is an evidence that relaxation occurs at least over minutes (Figure 7C, double arrow). Similar stretching and relaxation behaviors were observed with the other microscaffolds obtained in this study.

Microscaffolds Architecture. To investigate the architecture of the microscaffolds, dried samples attached to either the slide or the coverslip were recovered and imaged by AFM (Figure 8). The samples analyzed were assembled with an AC voltage of 1 V amplitude at a frequency of 1 kHz, 10 kHz (corresponding optical images in Figure 4) and 100 kHz. The DC bias was set to 100 mV for the first two frequencies and 500 mV for the last one. We observed two different surface morphologies, a dense meshwork of filaments with a diameter around 8−12 nm (Figure 8A, E, and F), and bundles with diameters ranging between 100 and 200 nm (Figure 8B−D). Single filaments are easily recognizable (Figure 8A, arrowheads and inset) and even form a quasi-regular mesh in some locations (Figure 8F, arrowheads). The bundles were generally straight (Figure 8B,C, arrows) and, in some occasions, they were seen to loop above the surface (Figure 8D, arrows). Due to the large size of the samples, we were not able to quantify the occurrence of the two types of morphology. We also observed large vimentin bundles when performing the same electric-field induced assembly experiments on a surface using micropatterned gold electrodes and sharp metal probes (Figure S1).

Discussion

In previous in vitro studies, the vimentin assembly pathway has been mainly characterized using electron microscopy or atomic force microscopy[10−12] at protein concentration around 0.1 mg/mL. Due to the fact that the end to end fusion of ULFs is the critical assembly steps as demonstrated recently by Kirmse and co-workers,[12] it is expected that increasing the protein concentration in a volume should have a dramatic impact on the assembly process. Because vimentin becomes insoluble in DP buffer above 5−10 mg/mL, the only way to access higher concentrations was ultracentrifugation above 50000 g. In this study we show that DEP combined with optical and atomic force microscopy allows to study vimentin assembly at concentrations close to the theoretical limit of 100 mg/mL.

The main result of this study is the demonstration that vimentin, in the assembly regime, can be induced by DEP to form dense microscaffolds that remain after removing the electric field. In the two facing cylinder geometry that we used, the nonuniform electric field is mainly due to the fringing fields at the sharp edges but we cannot completely neglect the influence of electrode surface roughness. Still it is clear from our data that the deposition of vimentin occurs always at the edges of the two wires (Figures 3−5). Furthermore, the growth

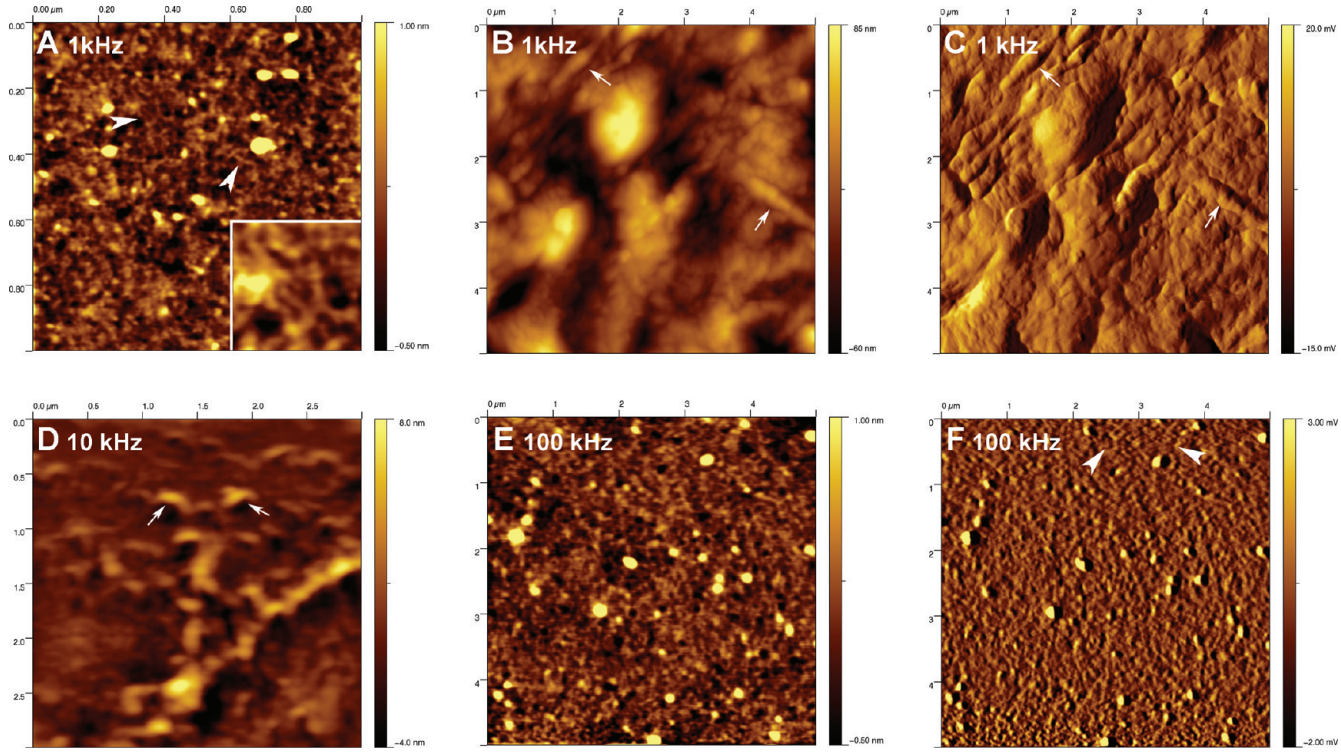

Figure 8. In some cases, the microscaffolds stuck to the glass and to the wire while drying. After removal of the wires, remnants of the dried microscaffolds were recovered washed with ultrapure water to remove salt deposits, dried again with nitrogen and imaged by atomic force microscopy (AFM) in contact mode. (A−C) Height and deflection images of the surface of a microscaffold obtained at 100 mV DC bias and an AC voltage of 1 V amplitude at 1 kHz. Two types of domains were observed. In (A) the surface is composed of a mesh of thin filaments 8−12 nm in diameter (arrowheads). Inset: blow-up of a small region of the image highlighting a few filaments. The area is 155 times 155 nm^2. In (B,C) the surface is composed of an array of large bundle 100−200 nm in diameter (arrows). (D) Height image of the surface of a microscaffold obtained at 100 mV DC bias and an AC voltage of 1 V amplitude at 10 kHz (see Figure 4). Filamentous bundles, 100 nm in diameter are seen looping out of the surface as in a loose fabric. (E,F) Height and deflection images of the surface of a microscaffold obtained at 500 mV DC bias and an AC voltage of 1 V amplitude at 100 kHz. The surface is a mesh of thin filaments (arrowheads) similar to the ones image in (A). Notice the quasi-regular quadratic network of overlapping filaments (arrowheads).

of the microscaffolds seem to follow the field lines of the fringing field (Figure 4A,B). Hence, the microscaffolds were always denser on the edges than in the center where the field is supposed to be more uniform (Figure 4B,C).

To understand the mechanism yielding such dense microscaffolds, one has to consider the role played by the DC and AC fields. In the case of the free ions in solution, their mobility is in the order of 10^{-8} $m^2 \cdot V^{-1} \cdot s^{-1}$.[23] If we consider a 1 V amplitude AC voltage over a 100 μm gap, we get a velocity of 100 μm/s for the ions. Which means that as long as the AC frequency is an order of magnitude higher than the characteristic frequency of the system, that is, 1 Hz, then most of the ions oscillate without reaching the electrodes. Superimposing a 100−500 mV DC bias to the AC field will allow the ions to drift slightly in one direction. As the DC bias is increased, more accumulation of ions is expected on both electrodes. This statement correlates with the fact that microscaffold growth was enhanced by increasing the DC bias. Still, in all our experiments, the AC frequency was always high enough with respect to the characteristic frequency of the ions to avoid a Helmoltz double layer at the electrodes and the cancellation of the electric-field in the solution.

The behavior of vimentin in our experiments is more complex because this protein is a slightly negatively charged polyelectrolyte at neutral pH, that is, 84 negative charges and 65 positive charges for only 466 amino-acids. Hence, vimentin in any of its forms along the assembly pathway to filaments (Figure 1) carries a cloud of at least a few hundred positive and negative ions. The vimentin structures are also anisotropic and are expected to be polarized under an electric field. Because mixing of the two solutions was complete within seconds in the flow chamber (see Materials and Methods), we can assume that vimentin assembly occurred everywhere in the chamber. This means that, as time goes, larger and larger vimentin structures have to be moved by the electric field. The weak DC field alone, around 10 $V \cdot cm^{-1}$, was not sufficient to induce microscaffold growth (Figure 3), indicating that the increase in net charge of the vimentin structures as they grew was not sufficient to counterbalance their volume increase. However, the DC field was necessary to direct the vimentin deposition on the positive electrode, indicating that the assembled vimentin structures are also negatively charged at neutral pH (Figures 3 and 5). In the presence of the AC field, the DEP force on the polarized vimentin structures increased as they grew,[24] thus yielding more deposition of vimentin around the electrodes than in the DC case alone (Figure 4).

Based on the optical micrographs (Figure 4B) and AFM images of the surface of some microscaffolds (Figure 8), we propose that the microscaffolds are dense three-dimensional networks of entangled vimentin filaments with a diameter of 8−12 nm that also contain large bundles with diameter in the 100−200 nm range. Stretching the microscaffolds by increasing the gap between the electrodes revealed single fibers that reached a length of around 500 μm without breaking (Figure 6C). We propose that these fibers are either formed by a group of aligned bundles or by drawing the network of vimentin filaments. In both cases, we expect the tensile properties of these fibers to be similar to those of Hagfish slime threads that are 1 μm wide

bundles of keratin-like filaments.[22] However, the extensibility of our vimentin fibers is at least double that of Hagfish slime threads.[22] First it is most probable that the bundles are curled or crimped within the microscaffolds thus giving the impression of extreme extensibility. Second, the constituents of the fibers, either single filaments or bundles, may slide past each other. Third, we recently proposed based on AFM measurements that the extensibility of single IFs is due to two mechanisms, an unfolding of each tetramers and a sliding of the tetramers past each others within the filaments.[20,25]

Conclusion

DEP is a powerful technique to manipulate molecules and particles in solution. We show in this study that the technique can also be employed to assemble web-like structures from fibrous proteins without the need of drying. The method should be applicable to other fibrous proteins than vimentin. For example, it could be used as an alternative method to form bundles or microspheres from silk recombinant proteins.[26,27] One of the possible applications of our approach is the ability to form microscaffolds with only a few micrograms of proteins that could potentially be used as seeds for the culture of larger grafts.

Acknowledgment. This work has been supported by NSERC through Discovery Grants awarded to L.K. and I.G.H. as well as through an USRA fellowship awarded to T.R.C.

Supporting Information Available. Video showing the experiment presented in Figure 4. The video is accelerated 10 times and starts 100 s after injection. Figure S1 presents the result of an assembly experiment performed in a different geometry. This material is available free of charge via the Internet at http://pubs.acs.org.

References and Notes

(1) Hoffman, P. D.; Sarangapani, P. S.; Zhu, Y. *Langmuir* 2008.
(2) Suzuki, M.; Yasukawa, T.; Shiku, H.; Matsue, T. *Biosens. Bioelectron.* **2008**, *24*, 1049–1053.
(3) Kua, C. H.; Lam, Y. C.; Rodriguez, I.; Yang, C.; Youcef-Toumi, K. *Anal. Chem.* **2008**, *80*, 5454–5461.
(4) Pohl, H. A.; Crane, J. S. *Biophys. J.* **1971**, *11*, 711–727.
(5) Kang, Y.; Li, D.; Kalams, S. A.; Eid, J. E. *Biomed. Microdevices* **2008**, *10*, 243–249.
(6) Eisenstadt, M.; Scheinberg, I. H. *Biopolymers* **1973**, *12*, 2491–2512.
(7) Lapizco-Encinas, B. H.; Rito-Palomares, M. *Electrophoresis* **2007**, *28*, 4521–4538.
(8) Lapizco-Encinas, B. H.; Ozuna-Chacon, S.; Rito-Palomares, M. *J. Chromatogr. A* **2008**, *1206*, 45–51.
(9) Cohen, C. *J. Struct. Biol.* **1998**, *122*, 3–16.
(10) Herrmann, H.; Haner, M.; Brettel, M.; Muller, S. A.; Goldie, K. N.; Fedtke, B.; Lustig, A.; Franke, W. W.; Aebi, U. *J. Mol. Biol.* **1996**, *264*, 933–953.
(11) Mucke, N.; Wedig, T.; Burer, A.; Marekov, L. N.; Steinert, P. M.; Langowski, J.; Aebi, U.; Herrmann, H. *J. Mol. Biol.* **2004**, *340*, 97–114.
(12) Kirmse, R.; Portet, S.; Mucke, N.; Aebi, U.; Herrmann, H.; Langowski, J. *J. Biol. Chem.* **2007**, *282*, 18563–18572.
(13) Sokolova, A. V.; Kreplak, L.; Wedig, T.; Mucke, N.; Svergun, D. I.; Herrmann, H.; Aebi, U.; Strelkov, S. V. *Proc. Natl. Acad. Sci. U.S.A.* **2006**, *103*, 16206–16211.
(14) Herrmann, H.; Hofmann, I.; Franke, W. W. *J. Mol. Biol.* **1992**, *223*, 637–650.
(15) Herrmann, H.; Aebi, U. *Cell. Mol. Life Sci.* **1999**, *55*, 1416–1431.
(16) Mucke, N.; Kreplak, L.; Kirmse, R.; Wedig, T.; Herrmann, H.; Aebi, U.; Langowski, J. *J. Mol. Biol.* **2004**, *335*, 1241–1250.
(17) Yamada, S.; Wirtz, D.; Coulombe, P. A. *Mol. Biol. Cell* **2002**, *13*, 382–391.
(18) Kreplak, L.; Aebi, U.; Herrmann, H. *Exp. Cell Res.* **2004**, *301*, 77–83.
(19) Strelkov, S. V.; Herrmann, H.; Aebi, U. *Bioessays* **2003**, *25*, 243–251.
(20) Kreplak, L.; Herrmann, H.; Aebi, U. *Biophys. J.* **2008**, *94*, 2790–2799.
(21) Kreplak, L.; Bar, H.; Leterrier, J. F.; Herrmann, H.; Aebi, U. *J. Mol. Biol.* **2005**, *354*, 569–577.
(22) Fudge, D. S.; Gardner, K. H.; Forsyth, V. T.; Riekel, C.; Gosline, J. M. *Biophys. J.* **2003**, *85*, 2015–2027.
(23) Lee, S. H.; Rasaiah, J. C. *J. Chem. Phys.* **1994**, *101*, 6964–6974.
(24) Pohl, H. A.; Crane, J. S. *J. Theor. Biol.* **1972**, *37*, 1–13.
(25) Kreplak, L.; Bar, H. *J. Mol. Biol.* **2009**, *385*, 1043–1051.
(26) Rammensee, S.; Slotta, U.; Scheibel, T.; Bausch, A. R. *Proc. Natl. Acad. Sci. U.S.A.* **2008**, *105*, 6590–6595.
(27) Slotta, U. K.; Rammensee, S.; Gorb, S.; Scheibel, T. *Angew. Chem., Int. Ed.* **2008**, *47*, 4592–4594.

BM900398N